Unified picture of cantilever frequency shift measurements of magnetic resonance

SangGap Lee, Eric W. Moore, and John A. Marohn*
Department of Chemistry and Chemical Biology, Cornell University, Ithaca, New York 14853, USA
(Received 22 December 2011; published 27 April 2012)

We report a unified framework describing all existing protocols for spin manipulation and signal creation in frequency-modulation magnetic resonance force microscopy using classical perturbation theory. The framework is well suited for studying the dependence of the frequency shift on the cantilever amplitude via numerical simulation. We demonstrate the formalism by recovering an exact result for a single spin signal and by simulating, for the first time as a function of cantilever amplitude, the frequency shift due to a volume of noninteracting spins inverted by an adiabatic rapid passage. We show that an optimal cantilever amplitude exists that maximizes the signal. Our findings suggest that understanding the amplitude dependence of the spin signal will be important for designing future high-sensitivity experiments.

DOI: 10.1103/PhysRevB.85.165447 PACS number(s): 76.60.−k, 76.30.−v, 07.79.Pk

I. INTRODUCTION

Magnetic resonance force microscopy[1–5] has achieved proton imaging at a resolution of 4 nm,[6] competitive with cryoelectron tomography[7,8] and ion-abrasion scanning electron microscopy.[9] The mechanical detection and imaging of electron spin resonance (ESR) from single defects in silica has been demonstrated;[10] recent advances suggest the feasibility of mapping the locations of individual nitroxide-based electron-spin labels in order to determine the tertiary structure of single biomolecules and macromolecular complexes.[11–14] The mechanical detection of ferromagnetic resonance[15–21] offers exciting possibilities for spectroscopically probing spin relaxation, interlayer coupling, and local internal fields in individual magnetic nanostructures. For many of these applications, detection of magnetic resonance as a spin-induced modulation of the eigenfrequency of a microcantilever offers many advantages. A number of seemingly disparate approaches to frequency-modulation magnetic resonance force microscopy (FM-MRFM) have been demonstrated experimentally[10,11,22–32] and considered theoretically.[33–43] The goals of this paper are to (1) unify the theoretical descriptions of these approaches into a single semiclassical formalism well suited for numerical calculations and (2) lift the small-cantilever-amplitude approximation limiting prior treatments of FM-MRFM. We demonstrate our signal-calculation approach by numerically calculating the FM-MRFM signal from an extended object and showing that the magnetic resonance signal is maximized at a finite cantilever amplitude.

In this paper we consider three FM-MRFM spin-manipulation and signal creation protocols. Each of these approaches places different requirements on the length of the sample's relaxation times ($T_{1\rho}$, the spin-lattice relaxation time in the rotating frame, and $T_1 \gg T_{1\rho}$, the spin-lattice relaxation time in the laboratory frame) relative to the cantilever period ($T = 1/f$, with f the cantilever resonance frequency). The first protocol considered here is the oscillating cantilever-driven adiabatic reversals or OSCAR protocol. In this protocol the cantilever frequency shift arises from a time-dependent, cantilever-synchronized *force* created by spin inversions induced jointly via the continuous application of microwaves or radiowaves and a modulated local field created by the oscillating cantilever. This protocol requires $T_{1\rho} \gg T$ and has been used to detect both ESR[10,22,23,30] and NMR.[25] The second protocol considered here is the cantilever-enabled readout of magnetization inversion transients or CERMIT protocol, in which a modulation of spin magnetization is induced by a short burst of microwaves or radiowaves and the resulting change in the *force gradient* acting on the cantilever tip shifts the cantilever's resonance frequency. The method has been used to detect NMR[24,28] and ESR[11,32] and requires only $T_1 \geqslant T$. A final set of FM-MRFM protocols considered here are those based on force gradients and cyclic saturation of sample magnetization, applicable to fast-relaxing spins with $T_1 \leqslant T$ and used so far to detect ESR.[26,27,29,31] These frequency-shift experiments are not obviously related; here we show that all three classes of experiments can nevertheless be described by a single unified formalism.

The need for the new formalism is clear. Unifying the description of all FM-MRFM signals into a single formalism paves the way for developing a program for numerically calculating the signal from an extended object for all possible frequency-shift experiments. While distinct first-principles derivations of both the OSCAR[33–35,39,43] and the CERMIT effect[11,24] have been reported, existing derivations all assume that the cantilever amplitude is much smaller that the tip-sample separation. Here we lift this small-amplitude approximation. Since working at finite cantilever amplitude is crucially important for optimizing the signal-to-noise ratio in a cantilever frequency-shift experiment,[44] our findings significantly advance our ability to design and optimize future experiments.

II. GENERAL ANALYTICAL FORMALISM

Our starting point for unifying the various FM-MRFM protocols is the following formula, developed by Giessibl[45] from Hamilton-Jacobi perturbation theory, for the shift in the resonance frequency Δf of a cantilever arising from a time-dependent force acting on the cantilever tip:

$$\Delta f = -\frac{f}{k q_{\mathrm{pk}}^2} \langle \vec{F}_{\mathrm{on\ tip}} \cdot \vec{q} \rangle_T. \tag{1}$$

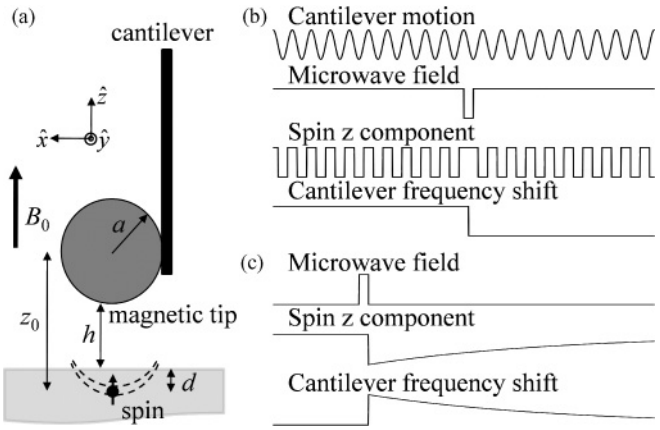

FIG. 1. Frequency-modulation magnetic resonance force microscopy of slowly relaxing spins. Schematic illustration of (a) the "hangdown" cantilever geometry, showing the cantilever with a magnetic tip and a spin buried in the extended sample, (b) the interrupted OSCAR spin manipulation and signal creation protocol, and (c) the CERMIT protocol.

Here f is the cantilever's resonance frequency, k is the cantilever's spring constant, $\vec{q} = \hat{q}\, q(t)$ is the tip position with $\hat{q}$ the unit vector parallel to the direction of cantilever oscillation and $q(t) = q_{\rm pk}\, \sin(2\pi f t)$, and $\vec{F}_{\rm on\ tip}$ is the time-dependent force acting on the tip. In Eq. (1), $\langle\,\rangle_T$ represents the temporal average taken over a single period of oscillation.

III. SINGLE-SPIN FREQUENCY-SHIFT SIGNALS IN THE SMALL-AMPLITUDE LIMIT

Let us begin by using Eq. (1) to describe the interrupted OSCAR, CERMIT, and cyclic saturation experiments in the limit where the cantilever amplitude is smaller than the tip-sample separation. We model the specific experimental configurations sketched in Figs. 1 and 2. The interrupted OSCAR experiment sketched in Figs. 1(a) and 1(b) is identical to the experiments of Refs. 10, 23, 25, and 30. The magnet-on-cantilever CERMIT experiment sketch in Figs. 1(a) and 1(c) is conceptually identical to the sample-on-cantilever CERMIT experiment of Ref. 28; the formalism developed below is

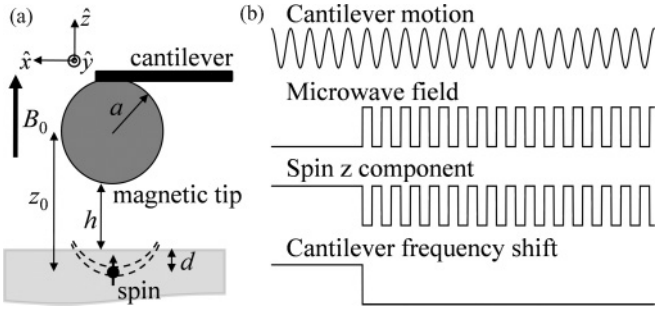

FIG. 2. Frequency-modulation magnetic resonance force microscopy of fast-relaxing spins. Schematic illustration of (a) the cantilever geometry and (b) the first-harmonic spin manipulation and signal creation protocol via cyclic saturation with $\phi = 0$ [see Eq. (10) and text].

easily modified to encompass the experiments of Refs. 11, 24, and 32 in which the field is applied in other orientations. The specific cyclic saturation experiment sketched in Fig. 2 is conceptually identical to the sample-on-cantilever experiments of Refs. 26, 27, and 29.

In the experiments of Figs. 1 and 2 we assume for simplicity that a uniform external magnetic field is applied along the z axis and that this external field is much larger than the tip field at any spin site in the sample. Within these approximations, the force of interaction between spins and the magnetic tip is given by

$$-\vec{F}_{\rm on\ tip} = \vec{F}_{\rm on\ spin} = \vec{\nabla}(\vec{m}_{\rm spin} \cdot \vec{B}_{\rm tip}) \simeq m^z_{\rm spin} \vec{\nabla} B^z_{\rm tip}. \quad (2)$$

Consequently,

$$\vec{F}_{\rm on\ tip}(t) \cdot \vec{q}\,(t) \simeq -m^z_{\rm spin}(t) \vec{\nabla} B^z_{\rm tip}(\vec{r} - \vec{q}\,(t)) \cdot \vec{q}\,(t)$$
$$= -m^z_{\rm spin}(t) \frac{\partial B^z_{\rm tip}}{\partial q}(\vec{r} - \hat{q}\, q(t))\, q(t), \quad (3)$$

with $\vec{r}$ the spin location relative to the center of the tip at equilibrium, $\vec{q} = 0$. Below we use Eqs. (1) and (3) to calculate the frequency shift expected from a CERMIT experiment carried out on an extended object and examine the dependence of the calculated signal on cantilever amplitude. Previous descriptions of FM-MRFM experiments follow from these equations in the limit that the cantilever amplitude goes to zero. Expanding $\partial B^z_{\rm tip}/\partial q$ in Eq. (3) in a Taylor series about $\vec{q} = 0$ yields, to first order,

$$\vec{F}_{\rm on\ tip} \cdot \vec{q} \approx -m^z_{\rm spin}(t) \left\{ \frac{\partial B^z_{\rm tip}}{\partial q}(\vec{r}) - q(t) \frac{\partial^2 B^z_{\rm tip}}{\partial q^2}(\vec{r}) \right\} q(t), \quad (4)$$

where we have used the approximation that the cantilever amplitude is small compared to the tip-spin separation, $|q(t)| \ll \|\vec{r}\|$. The zero-order term in the series is force related while the first-order term is force-gradient related. What is learned from this development is that the cantilever frequency shift in general depends on both the force *and* the force gradient, the two terms arising from a Taylor expansion of the underlying exact results of Eqs. (1) and (3).

To calculate the frequency shift in the three FM-MRFM experiments of Figs. 1 and 2, it remains to enumerate the exact spin-modulation protocols used in each method. In the interrupted OSCAR experiment of Figs. 1(a) and 1(b) the sample magnetization is modulated during a cantilever period T as follows:

$$m^z_{\rm spin} = \begin{cases} \text{lock} & \text{antilock} & \text{duration} \\ -\mu & +\mu & 0 \leqslant t < T/2, \\ +\mu & -\mu & T/2 \leqslant t < T, \end{cases} \quad (5)$$

where μ is the spin magnetic moment, decaying with a time constant $T_{1\rho}$. In order to compute the signal, let us assume that $T \ll T_{1\rho}$, so that $m^z_{\rm spin}(t+T) = m^z_{\rm spin}(t)$. Inserting Eq. (5) into Eq. (4), inserting the result into Eq. (1), and taking the temporal average gives

$$\Delta f_{\rm OSCAR} = \mp \frac{2 f \mu}{\pi k x_{\rm pk}} \frac{\partial B^z_{\rm tip}}{\partial x}(\vec{r}) \quad \left\{ \begin{matrix} \text{lock} \\ \text{antilock} \end{matrix} \right\}, \quad (6)$$

where we have used $q(t) = x_{\rm pk}\, \sin(2\pi f t)$. This result agrees with the result asserted by Mamin *et al.* in Ref. 23 and derived

from first principles by Berman *et al.* in Ref. 43. Only the *force*-based term in Eq. (4) survives in the OSCAR protocol.

In the CERMIT experiment, Figs. 1(a) and 1(c), the magnetization immediately following the application of the oscillating magnetic field is

$$m^z_{\rm spin}(t) = \mu, \tag{7}$$

decaying with a time constant T_1 which we assume is much longer than T. Substituting Eq. (7) into Eq. (4), inserting the result into Eq. (1), and taking the temporal average gives

$$\Delta f_{\rm CERMIT} = -\frac{f\mu}{2k}\frac{\partial^2 B^z_{\rm tip}}{\partial x^2}(\vec{r}). \tag{8}$$

This result is equivalent to the result presented by Garner *et al.* in Ref. 24. Only the *force gradient*–based term in Eq. (4) survives in the CERMIT protocol.

In the cyclic-saturation protocol of Fig. 2, the strength of the microwave field is modulated between $B_1^{\rm lo}$ and $B_1^{\rm hi}$ every cantilever half period. Assuming $T_1 \ll T$, the magnetic moment is given by

$$m^z_{\rm spin}(t) = \begin{cases} A(z-q(t))\Delta z M^z_{B_1^{\rm lo}}, & 0 \leqslant t < T/2 \\ A(z-q(t))\Delta z M^z_{B_1^{\rm hi}}, & T/2 \leqslant t < T, \end{cases} \tag{9}$$

where A is the area of spins in resonance, Δz is the thickness of the resonant shell, $M^z_{B_1^{\rm lo}}$ is the spin magnetization in the (microwaves-off) fully polarized state, and $M^z_{B_1^{\rm hi}}$ is the spin magnetization in the (microwaves-on) saturated state. The cantilever displacement in Fig. 2 is given by $q(t) = z_{\rm pk}\sin(2\pi f t - \phi)$ so that the spin magnetization is modulated with a phase of ϕ with respect to the cantilever oscillation. Inserting Eq. (9) into Eq. (4) ultimately yields

$$\begin{aligned}\Delta f_{\rm cyc\ sat} = -\frac{f}{k}\frac{\Delta z}{}\Bigg\{ & -\cos\phi\,\frac{\delta M_z\, A}{\pi\, z_{\rm pk}}\frac{\partial B^z_{\rm tip}}{\partial z}(\vec{r}) \\ & + \frac{\Sigma M_z}{4}\frac{\partial A}{\partial z}\frac{\partial B^z_{\rm tip}}{\partial z}(\vec{r}) + \frac{\Sigma M_z\, A}{4}\frac{\partial^2 B^z_{\rm tip}}{\partial z^2}(\vec{r}) \\ & + \left(\frac{\cos 3\phi}{3} - 3\cos\phi\right)\frac{\delta M_z\, z_{\rm pk}}{4\pi}\frac{\partial A}{\partial z}\frac{\partial^2 B^z_{\rm tip}}{\partial z^2}(\vec{r})\Bigg\},\end{aligned} \tag{10}$$

with $\delta M_z = M^z_{B_1^{\rm lo}} - M^z_{B_1^{\rm hi}}$ and $\Sigma M_z = M^z_{B_1^{\rm lo}} + M^z_{B_1^{\rm hi}}$. We conclude that both the *force* and *force gradient* terms in Eq. (4) survive the *cyclic saturation* protocol. The first term in Eq. (10) dominates in the limit of strong microwaves and $A/z_{\rm pk} \gg \partial A/\partial z$, which holds true when the microwaves are in resonance with spins in the middle of a comparatively homogeneous sample. The first term in Eq. (10) is the result derived by Lee *et al.* in Ref. 29 with $\phi = 0$. The second and third terms in Eq. (10) contribute to the signal as long as the microwaves are on, whether unmodulated as in the experiment of Ref. 26 or modulated anharmonically as in the experiment of Ref. 31. It is notable that the second term in Eq. (10) contributes to the signal only when microwaves are in resonance with spins at the surface of a thin-filmed spin sample where $\partial A/\partial z$ becomes large. The fourth term in Eq. (10) is negligible when $z_{\rm pk}$ is much smaller than the magnet diameter, which has been the case in all cyclic-saturation FM-MRFM experiments carried out to date.

IV. SINGLE-SPIN FREQUENCY-SHIFT CERMIT SIGNAL IN THE FINITE-AMPLITUDE LIMIT

So far we have shown that Eqs. (6), (8), and (10) all follow from Eq. (1) in the small-cantilever-amplitude limit. Optimizing the signal-to-noise ratio in an FM-MRFM experiment, however, demands carrying out experiments at finite cantilever amplitude. There are several ways that one might imagine deriving the full cantilever-amplitude dependence of the FM-MRFM signal. One way would be to start with the equations of motion for the cantilever-spin system and directly integrate them. Although this would successfully capture the relevant result, it would be difficult, time consuming, and error prone. A better approach is to numerically integrate in Eq. (1), as we now show.

Let us illustrate using Eq. (1) to numerically compute the signal in an FM-MRFM experiment by calculating the signal in a CERMIT experiment carried out at finite cantilever amplitude on both single-spin and extended samples. For a single spin located directly below the tip, $\vec{r} = (0,0,z)$ and the necessary integration can be carried out analytically. For a spherical tip in the geometry of Fig. 1(a), the integration of Eq. (1) involves only the x component of the force. For a spin directly below the tip, the x component of the force is given by

$$F_{{\rm on\ tip},x} = -\mu\frac{\partial B^z_{\rm tip}}{\partial x} \tag{11}$$

$$= -\mu\mu_0 M_{\rm tip} a^3 \frac{x(t)^3 - 4z^2 x(t)}{[z^2 + x(t)^2]^{7/2}} \tag{12}$$

with $x(t) = -x_{\rm pk}\cos(2\pi f t)$, a the tip radius, and $M_{\rm tip}$ the tip magnetization. Inserting Eq. (12) into Eq. (1) and carrying out the resulting integral, we find

$$\Delta f = -\frac{f}{2k x_{\rm pk}}\frac{\mu\mu_0 M_{\rm tip}}{a}\left(\frac{a}{z}\right)^4 I\left(\frac{z}{x_{\rm pk}}\right), \tag{13}$$

where

$$\begin{aligned} I(Z) = \frac{Z^3}{3\pi(Z^2+1)^3}\Bigg\{ & 4(2Z^4 - 7Z^2 - 1)\,E\left(-\frac{1}{Z^2}\right) \\ & - 8(Z^4 - 1)K\left(-\frac{1}{Z^2}\right)\Bigg\}\end{aligned} \tag{14}$$

with $K(m)$ and $E(m)$ the complete elliptic integrals of the first and second kind, respectively, and $Z = z/x_{\rm pk}$ the ratio of the tip-sample separation to the tip amplitude.[5]

In the limit that the tip amplitude goes to zero, $x_{\rm pk} \to 0$ and $x_{\rm pk}^{-1} I(z/x_{\rm pk}) \to -4/z + O(x_{\rm pk}^2)$. To leading order

$$\Delta f \approx \frac{f}{2k}\frac{4\mu\mu_0 M_{\rm tip} a^3}{z^5}, \tag{15}$$

which agrees with Eq. (8), taking $B^z_{\rm tip}$ for a spherical tip. So although Eq. (12) involves the first derivative of the tip field $\partial B^z_{\rm tip}/\partial x$, according to Eqs. (8) and (15) the frequency shift is proportional to the second derivative of the tip field $\partial^2 B^z_{\rm tip}/\partial x^2$ at small amplitude.

Let us consider adjusting the radius of the magnetic tip to optimize the CERMIT signal. Take $z = h + a$, with h the

tip-sample separation, and let $d = 0$ for simplicity. Optimizing Δf in Eq. (15) with respect to a yields $a_{\rm opt} = 3h/2$ for the optimal tip radius in a small-amplitude force-gradient experiment. This result differs from the optimal tip radius of $a_{\rm opt} = 3h$ derived by Sidles *et al.*[4] for a force-based experiment.

In an experiment, however, one must optimize not the signal but the signal-to-noise ratio (SNR). Because the frequency noise decreases with increasing cantilever amplitude, to optimize the SNR in a single-spin experiment we need to calculate the signal using Eq. (13). Let us assume that the frequency noise is thermally limited, with a power spectrum given by[44,46]

$$P_{\delta f}^{\rm th} = \frac{k_b T}{\pi^2 k x_{\rm pk}^2 \tau_0}, \tag{16}$$

with k_b Boltzmann's constant, T temperature, and τ_0 the cantilever ring-down time. The SNR is

$$\mathrm{SNR}_{\Delta f} = \frac{\Delta f}{\left(P_{\delta f}^{\rm th} b\right)^{1/2}}, \tag{17}$$

with b the measurement bandwidth. Let us convert the frequency shift to an effective spring constant using $\Delta k = 2k\Delta f/f$. Substituting Eq. (16) into Eq. (17) yields

$$\mathrm{SNR}_{\Delta f} = \frac{f}{2k}\left(\frac{\pi^2 k \tau_0}{k_b T b}\right)^{1/2} \underbrace{\Delta k\, x_{\rm pk}}_{\Delta F_{\rm eff}}. \tag{18}$$

The underbraced term is an effective force. The effective force associated with the single-spin frequency-shift signal of Eq. (13) is

$$\Delta F_{\rm eff} = -\frac{\mu\mu_0 M_{\rm tip}}{a}\left(\frac{a}{z}\right)^4 I\left(\frac{z}{x_{\rm pk}}\right). \tag{19}$$

We find that $\Delta F_{\rm eff}$, and therefore $\mathrm{SNR}_{\Delta f}$, is optimized at $x_{\rm pk}^{\rm opt} = 0.47z$ and $a_{\rm opt} = 3h$. The effective force is plotted in Fig. 3 as a function of $x_{\rm pk}$ and a for a nickel tip ($\mu_0 M_{\rm tip} = 0.6$ T) interacting with a single electron at a tip-sample separation of $h = 25$ nm. Interestingly, the radius which optimizes the SNR in a force-gradient experiment is $3h$ and not $3h/2$.

In the following section we calculate the frequency-shift signal for various experiments. As above, we present our results in terms of an effective force $\Delta F_{\rm eff} = \Delta k x_{\rm pk}$. The signal presented in this way is independent of cantilever spring constant and frequency. Moreover, optimizing $\Delta F_{\rm eff}$ (not Δf) will maximize the signal-to-noise ratio.

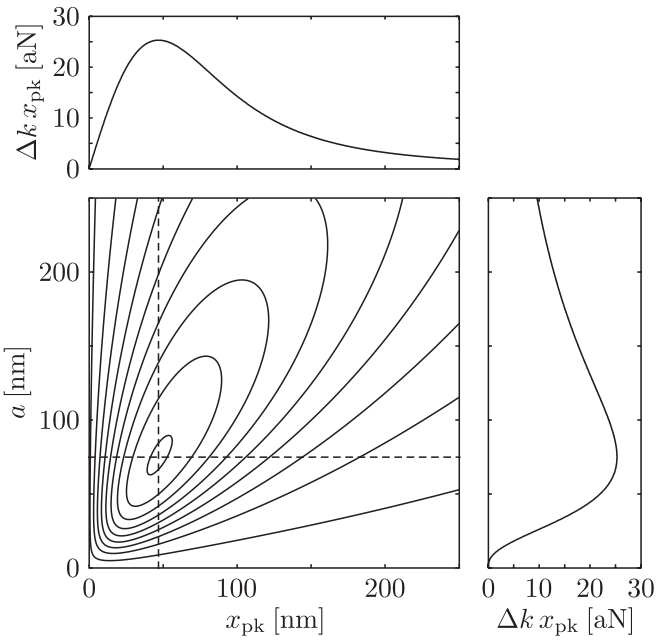

FIG. 3. Plot of the Eq. (19) effective force on a cantilever from a single spin located at a distance $h = 25$ nm below the surface of the cantilever's spherical nickel tip. The central plot presents contours of constant effective force, $\Delta F_{\rm eff} = \Delta k x_{\rm pk}$, as a function of tip radius a and cantilever amplitude $x_{\rm pk}$. The contours range from $\Delta k\, x_{\rm pk} = 1$ to 25 aN in steps of 3 aN. Slices through the effective-force surface are shown in the upper plot and right plot for $x_{\rm pk} = 47$ nm and $a = 75$ nm, respectively. The slice positions are indicated by dashed lines in the contour plot (left).

V. NUMERICAL CALCULATIONS

The frequency shift due to a spin located at an arbitrary location $\vec{r} = (x,y,z)$ is computed by substituting $x(t) = x - x_{\rm pk}\cos(2\pi f t)$ in the tip-field derivative in Eq. (11). The resulting Eq. (1) integral can be expressed in terms of an integral over an angle variable θ:

$$\Delta f = -\frac{f}{2\pi k x_{\rm pk}^2}\int_{-\pi}^{+\pi} \mu(x,y,z,\theta) \times \frac{\partial B_{\rm tip}^z(x - x_{\rm pk}\cos\theta, y, z)}{\partial x} x_{\rm pk}\cos\theta\, d\theta. \tag{20}$$

This integral must be computed numerically and summed over all spins in the sample. In the cantilever-synchronized OSCAR and cyclic-saturation FM-MRFM protocols, the spin magnetic moment μ depends parametrically on cantilever position through the local magnetic field. In all of the numerical calculations discussed below, the integral in Eq. (20) was approximated using 41 points and the trapezoid rule.

To begin, a numerical calculation was carried out for a single electron spin located at $\vec{r} = (0,0,75\ \text{nm})$ directly below a spherical nickel tip of radius $a = 50$ nm and magnetization $\mu_0 M_{\rm tip} = 0.6$ T. The calculated single-electron CERMIT signal is plotted as a function of the cantilever amplitude on the left-hand axis of Fig. 4. The calculated frequency-shift signal is expressed as an effective force. The numerical result agrees with the exact analytical result of Eqs. (13) and (19) to within a relative error of better than 1 part in 10^5, indicating that our simulation code is performing as expected.

Numerical calculations of the CERMIT signal were next carried out for an extended sample chosen to mimic the nitroxide radical sample of Ref. 11. Sample magnetization density was computed using the Curie law, assuming a spin density of $\rho = 2.41 \times 10^{25}$ m^{-3}, a sample temperature of $T = 4.2$ K, an electron g-factor of $g = 2.00572$ (the average g value of tempamine[47]), and a polarizing field of 0.62 T. The sample had dimensions $L_x = 1$ μm, $L_y = 1$ μm, $L_z = 0.25$ μm, and was approximated by a grid with the following numbers of points in each dimension: $N_x = 300$, $N_y = 550$, and $N_z = 80$. When summing Eq. (20) over spins in the

sample, only one half of the y dimension was contained in the sample mesh; the full-scale signal was recovered by scaling the simulated signal by 2. A spherical magnetic tip with radius $a = 25$ nm and magnetization $\mu_0 M_{\rm tip} = 0.6$ T located at $h = 25$ nm was used. Bloch equations with $T_1 = 1$ ms and $T_2 = 0.45$ μs were used to calculate μ as a function of the tip field, longitudinal applied field B_0, and the applied transverse microwave magnetic field amplitude B_1 and frequency $f_{\rm MW}$.

In this simulation we first assume that the sample spins are flipped via adiabatic rapid passage before the cantilever motion is initiated; in this case, μ in Eq. (20) is time independent. Immediately following the frequency-chirped microwave pulse, we assume that the cantilever is driven to a large amplitude, for instance by a voltage pulse to a nearby wire. The difference between the cantilever's spring constant before and after the microwave pulse will be the signal. Carrying out the numerical experiment in this way allows us to independently adjust the cantilever amplitude and the volume of spins contributing to the signal in order to isolate and understand the dependence of the frequency-shift signal on the cantilever amplitude.

The CERMIT signal was computed for two distributions or "sensitive slices" of inverted spin magnetization created by a frequency-chirped microwave pulse. The slices were created by applying an adiabatic rapid passage of center frequency $f_{\rm MW} = 17.5$ GHz and width $\Delta B = 1$ mT $= 28$ MHz$/\gamma_e$ in an external field of $B_0 = 0.6973$ T and 0.6710 T for slice 1 and slice 2, respectively. The sensitive slices are plotted to scale in the inset of Fig. 4, where shading has been used to indicate spins whose magnetization changed by 5% or more due to the rapid passage, $\Delta\mu/\mu_{\rm initial} \geqslant 0.05$. Slice 1 was chosen to give a signal analogous to the "local peak" of Ref. 11; the apparent slice radius, measured from the front edge of the magnet, is $r = 53.7$ nm and the slice depth, measured from the sample surface to the upper edge of the slice, was $d = 25.3$ nm. Slice 2 had a radius of $r = 84.0$ nm and a depth of $d = 53.8$ nm.

The calculated CERMIT signal for the two slices is plotted as a function of the cantilever amplitude on the right-hand axis of Fig. 4. The signal from slice 1 (solid circles) reaches a maximum at $x_{\rm pk} = 65$ nm, whereas the signal from slice 2 (solid triangles) reaches a maximum at $x_{\rm pk} = 100$ nm. Interestingly, the slice 2 signal is smaller than the slice 1 signal at small amplitudes but becomes larger than the slice 1 signal at large cantilever amplitudes, $x_{\rm pk} \geqslant 45$ nm. These results establish that the CERMIT signal is optimized at a

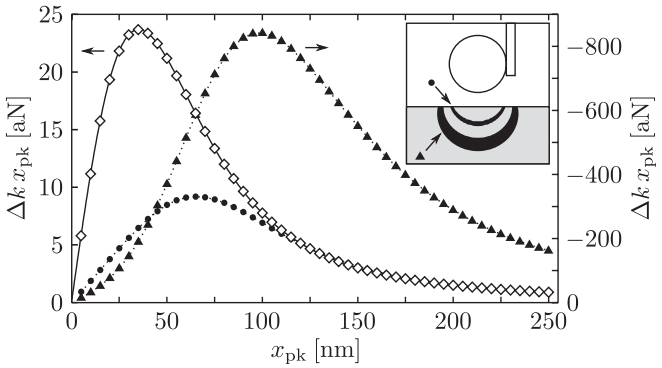

FIG. 4. Numerical simulation of frequency-shift CERMIT magnetic resonance signals using Eq. (20), with spins flipped prior to cantilever motion via an adiabatic frequency sweep. Left axis: Exact analytic result [solid line; Eq. (19)] and a numerical simulation (open diamonds) of the signal from a single electron spin located 25 nm directly below the magnetic tip's front edge. Right axis: Numerically simulated electron spin resonance signal from two sensitive slices of inverted magnetization (inset) from a semi-infinite sample of a 40-mM nitroxide radical at $T = 4.2$ K in resonance with 17.5-GHz microwaves. Simulation parameters: tip radius $a = 50$ nm, tip magnetization $\mu_0 M_{\rm tip} = 0.6$ T, and tip-sample separation $h = 25$; sample parameters are given in the text.

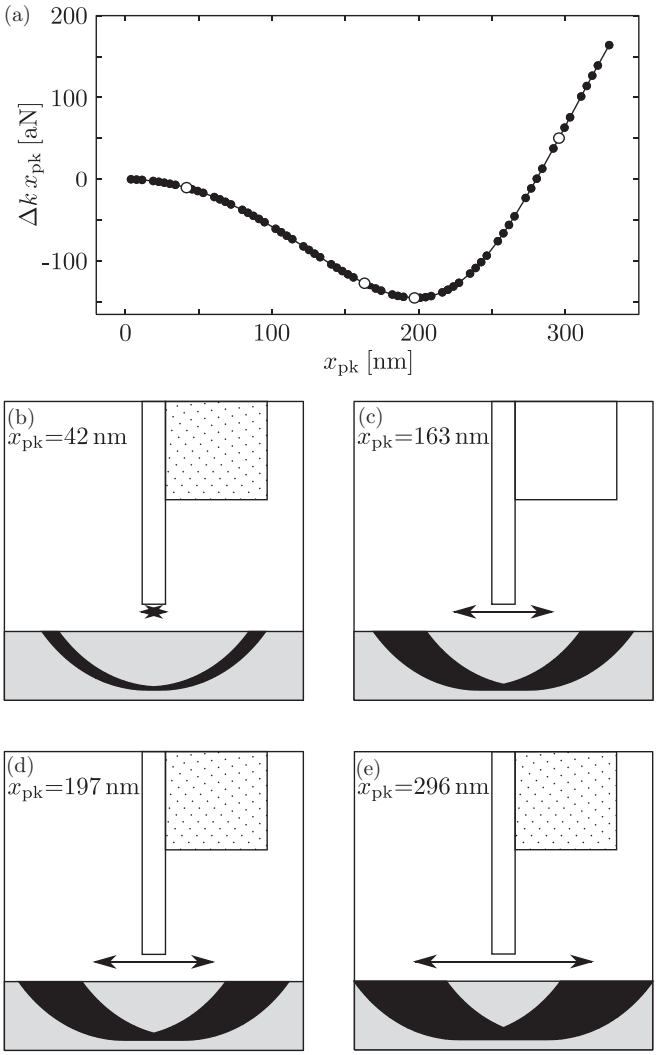

FIG. 5. Numerical simulation of frequency-shift CERMIT magnetic resonance signals using Eq. (20). Spins were flipped via continuous application of fixed-frequency microwaves during cantilever motion. (a) Electron-spin resonance signal simulated at selected cantilever amplitudes. The solid line is a guide to the eye. (b–e) Scale diagrams of the simulated sensitive slices for four cantilever amplitudes indicated by unfilled circles in (a): $x_{\rm pk} = 42$, 163, 197, and 296 nm. The overhanging nickel magnet is shown as a white rectangle and the silicon body of the cantilever as a dotted rectangle, the sample film is colored light gray, and the sensitive slice is colored black as in Fig. 4. The arrow indicates the cantilever's position at either extrema of its motion. See text for simulation parameters.

finite cantilever amplitude which is proportional to, but not exactly equal to, the effective radius of the sensitive slice.

Using adiabatic rapid passage to invert the electron-spin magnetization of a nitroxide radical is experimentally challenging because of the hardware required to deliver a frequency-chirped pulse and because of the large-amplitude ($B_1 \gg 0.1$ mT) transverse magnetic field needed to maintain the adiabatic condition. Moore *et al*. have demonstrated using spin saturation to create a large CERMIT signal.[11] In their experiment, large regions of saturated magnetization were created below the cantilever tip using the time-dependent local field provided by the moving cantilever in conjunction with irradiation by fixed-frequency small-amplitude ($B_1 \sim \mu$T) microwaves. We have used Eq. (20) to simulate the cantilever frequency shift in such an experiment.

The simulation assumed the cantilever-sample geometry of Fig. 1(a). The external polarizing field was, however, applied along the y axis as in the experiments of Refs. 11, 12, and 24 rather than along the z axis as depicted in Fig. 1. The magnetic field below the tip was calculated by modeling the tip as a uniformly magnetized nickel prism having magnetization $\mu_0 M_{\rm tip} = 0.6$ T and dimensions $l_x = 78$ nm, $l_y = 78$ nm, and $l_z = 1478$ nm. The sample had dimensions $L_x = 2.5$ μm, $L_y = 1.25$ μm, and $L_z = 0.23$ μm and was approximated by a grid with the following number of points in each dimension: $N_x = 1320$, $N_y = 330$, and $N_z = 95$. A tip-sample separation of $h = 91$ nm was used. To calculate spin magnetization, we set $f_{\rm MW} = 17.6$ GHz, $B_0 = 0.6287$ T, and $B_1 = 0.3$ μT. These simulation parameters were chosen to mimic the experiment of Ref. 12.

The simulated signal as a function of cantilever amplitude $x_{\rm pk}$ is shown in Fig. 5(a). In contrast with the results of Fig. 4, at low amplitude the signal rises supralinearly as $x_{\rm pk}$ is increased. This rise is accounted for by considering the change in the volume of saturated spins that results from increasing the cantilever amplitude. As in Fig. 4, the signal reaches a maximum as $x_{\rm pk}$ increases, but now the signal changes sign at large amplitude. To understand this new behavior, it is helpful to consider the scale diagrams of the cantilever and spin magnetization shown in Figs. 5(b)–5(e). When the cantilever amplitude is smaller than the inner radius $r_{\rm slice}^{\rm inner}$ of the sensitive slice, as in Figs. 5(b) and 5(c), the effective force is negative and there is a net outward force on the cantilever. As the cantilever amplitude is increased, Fig. 5(d), the effective force reaches a peak of $\Delta k x_{\rm pk} = -144.9$ aN at an amplitude of $x_{\rm pk} = 197$ nm, which is just slightly less than $r_{\rm slice}^{\rm inner} = 211$ nm. As the cantilever amplitude is further increased the net force decreases because of cancellation between regions of positive and negative $\partial^2 B_{\rm tip}^y / \partial x^2$, until at $x_{\rm pk} = 280$ nm the effective force becomes zero and $x_{\rm pk} \approx r_{\rm slice}^{\rm inner}$. With the cantilever amplitude increased to $x_{\rm pk} = 296$ nm, as in Fig. 5(e), $x_{\rm pk} > r_{\rm slice}^{\rm inner}$ and the signal becomes positive. The effective force continues to be positive and grows nearly linearly until the largest simulated cantilever amplitude of $x_{\rm pk} = 330$ nm.

Comparing the results of Figs. 4 and 5(a), we see that the peaking of the signal at finite cantilever amplitude is a general feature of the CERMIT signal. The behavior of the signal at small and large cantilever amplitudes, however, is quite sensitive to the spin-modulation details.

VI. CONCLUSIONS

We have presented a unified treatment of three distinct frequency-modulation MRFM protocols. The formalism relieves the finite-cantilever-amplitude approximation limiting previous descriptions of FM-MRFM experiments and is well adapted for numerical calculations. We have used the new formalism to numerically compute the signal for both single spin and extended samples. These simulations demonstrate that the signal in a CERMIT experiment is optimized at a finite cantilever amplitude. Although we have only simulated CERMIT experiments, we believe this to be a general finding and that any FM-MRFM protocol will produce a peak frequency shift at a finite cantilever amplitude. Experimental evidence of this expectation for interrupted OSCAR can be seen in the experiments described in Ref. 25, where signal magnitude versus cantilever amplitude curves were measured and were qualitatively similar to those shown in Fig. 4. This finding, in combination with the general result of Eq. (20), will be useful in designing and optimizing MRFM experiments including virus-scale proton imaging[6] and proposed single-electron-spin MRFM experiments on spin-labeled biomolecules.[11–14]

ACKNOWLEDGMENTS

S.L., E.W.M., and J.A.M. acknowledge funding from the National Institutes of Health (NIH NIGMS Grant No. 5R01GM-070012) and J.A.M acknowledges funding from the Army Research Office Multidisciplinary University Research Initiative (ARO MURI Grant No. W911NF-05-1-0403). We acknowledge useful discussions with Lee E. Harrell.

*jam99@cornell.edu

[1] J. A. Sidles, Appl. Phys. Lett. **58**, 2854 (1991).
[2] D. Rugar, C. S. Yannoni, and J. A. Sidles, Nature (London) **360**, 563 (1992).
[3] D. Rugar, O. Züger, S. Hoen, C. S. Yannoni, H.-M. Vieth, and R. D. Kendrick, Science **264**, 1560 (1994).
[4] J. Sidles, J. Garbini, K. Bruland, D. Rugar, O. Züger, S. Hoen, and C. Yannoni, Rev. Mod. Phys. **67**, 249 (1995).
[5] S. Kuehn, S. A. Hickman, and J. A. Marohn, J. Chem. Phys. **128**, 052208 (2008).
[6] C. L. Degen, M. Poggio, H. J. Mamin, C. T. Rettner, and D. Rugar, Proc. Natl. Acad. Sci. USA **106**, 1313 (2009).
[7] R. McIntosh, D. Nicastro, and D. Mastronarde, Trends Cell Biol. **15**, 43 (2005).
[8] A. Mader, N. Elad, and O. Medalia, Meth. Enzymology **483**, 245 (2010).
[9] J. A. Heymann, D. Shi, S. Kim, D. Bliss, J. L. Milne, and S. Subramaniam, J. Struct. Biol. **166**, 1 (2009).
[10] D. Rugar, R. Budakian, H. J. Mamin, and B. W. Chui, Nature (London) **430**, 329 (2004).

[11]E. W. Moore, S.-G. Lee, S. A. Hickman, S. J. Wright, L. E. Harrell, P. P. Borbat, J. H. Freed, and J. A. Marohn, Proc. Natl. Acad. Sci. USA **106**, 22251 (2009).
[12]S. A. Hickman, E. W. Moore, S.-G. Lee, J. G. Longenecker, S. J. Wright, L. E. Harrell, and J. A. Marohn, ACS Nano **4**, 7141 (2010).
[13]E. W. Moore, S.-G. Lee, S. A. Hickman, L. E. Harrell, and J. A. Marohn, Appl. Phys. Lett. **97**, 044105 (2010).
[14]J. G. Longenecker, E. W. Moore, and J. A. Marohn, J. Vac. Sci. Technol. B **29**, 032001 (2011).
[15]Z. Zhang, P. C. Hammel, and P. E. Wigen, Appl. Phys. Lett. **68**, 2005 (1996).
[16]O. Klein, V. Charbois, V. V. Naletov, and C. Fermon, Phys. Rev. B **67**, 220407 (2003).
[17]G. de Loubens, V. V. Naletov, O. Klein, J. B. Youssef, F. Boust, and N. Vukadinovic, Phys. Rev. Lett. **98**, 127601 (2007).
[18]G. de Loubens, V. V. Naletov, M. Viret, O. Klein, H. Hurdequint, J. B. Youssef, F. Boust, and N. Vukadinovic, J. Appl. Phys. **101**, 09F514 (2007).
[19]Y. Obukhov, D. Pelekhov, J. Kim, P. Banerjee, I. Martin, E. Nazaretski, R. Movshovich, S. An, T. Gramila, S. Batra *et al.*, Phys. Rev. Lett. **100**, 197601 (2008).
[20]O. Klein, G. de Loubens, V. V. Naletov, F. Boust, T. Guillet, H. Hurdequint, A. Leksikov, A. N. Slavin, V. S. Tiberkevich, and N. Vukadinovic, Phys. Rev. B **78**, 144410 (2008).
[21]I. Lee, Y. Obukhov, G. Xiang, A. Hauser, F. Yang, P. Banerjee, D. V. Pelekhov, and P. C. Hammel, Nature (London) **466**, 845 (2010).
[22]B. C. Stipe, H. J. Mamin, C. S. Yannoni, T. D. Stowe, T. W. Kenny, and D. Rugar, Phys. Rev. Lett. **87**, 277602 (2001).
[23]H. J. Mamin, R. Budakian, B. W. Chui, and D. Rugar, Phys. Rev. Lett. **91**, 207604 (2003).
[24]S. R. Garner, S. Kuehn, J. M. Dawlaty, N. E. Jenkins, and J. A. Marohn, Appl. Phys. Lett. **84**, 5091 (2004).
[25]H. J. Mamin, R. Budakian, B. W. Chui, and D. Rugar, Phys. Rev. B **72**, 024413 (2005).
[26]N. E. Jenkins, Ph.D. thesis, Cornell University, Ithaca, New York, 2007.
[27]Y. Obukhov, K. C. Fong, D. Daughton, and P. C. Hammel, J. Appl. Phys. **101**, 034315 (2007).
[28]H. J. Mamin, M. Poggio, C. L. Degen, and D. Rugar, Nat. Nanotechnol. **2**, 301 (2007).
[29]S.-G. Lee, S. Won, S.-b. Saun, and S. Lee, Nanotechnology **18**, 375505 (2007).
[30]K. C. Fong, P. Banerjee, Y. Obukhov, D. V. Pelekhov, and P. C. Hammel, Appl. Phys. Lett. **93**, 012506 (2008).
[31]K. Inomata, S. Tsuji, Y. Yoshinari, H. S. Park, and D. Shindo, J. Phys. Soc. Jpn. **78**, 033602 (2009).
[32]A. Vinante, L. Schinkelshoek, O. Usenko, G. Wijts, and T. Oosterkamp, Nat. Commun. **2**, 572 (2011).
[33]G. P. Berman, D. I. Kamenev, and V. I. Tsifrinovich, Phys. Rev. A **66**, 023405 (2002).
[34]G. P. Berman, V. N. Gorshkov, D. Rugar, and V. I. Tsifrinovich, Phys. Rev. B **68**, 094402 (2003).
[35]G. P. Berman, V. N. Gorshkova, and V. I. Tsifrinovich, Phys. Lett. A **318**, 584 (2003).
[36]G. P. Berman, F. Borgonovi, Z. Rinkevicius, and V. I. Tsifrinovich, Superlattices Microstruct. **34**, 509 (2003).
[37]G. P. Berman, F. Borgonovi, and V. I. Tsifrinovich, Quantum Inf. Comput. **4**, 102 (2004).
[38]G. P. Berman, F. Borgonovi, and V. I. Tsifrinovich, Phys. Lett. A **331**, 187 (2004).
[39]G. P. Berman, V. N. Gorshkov, and V. I. Tsifrinovich, J. Appl. Phys. **96**, 5081 (2004).
[40]G. P. Berman, F. Borgonovi, V. N. Gorshkov, and V. I. Tsifrinovich, IEEE Trans. Nanotechnol. **4**, 14 (2005).
[41]S. Mancini, D. Vitali, and H. Moya-Cessa, Phys. Rev. B **71**, 054406 (2005).
[42]G. P. Berman, F. Borgonovi, and V. I. Tsifrinovich, Phys. Lett. A **337**, 161 (2005).
[43]G. P. Berman, F. Borgonovi, and V. I. Tsifrinovich, Phys. Rev. B **72**, 224406 (2005).
[44]T. R. Albrecht, P. Grütter, D. Horne, and D. Rugar, J. Appl. Phys. **69**, 668 (1991).
[45]F. J. Giessibl, Phys. Rev. B **56**, 16010 (1997).
[46]S. Yazdanian, J. Marohn, and R. Loring, J. Chem. Phys. **128**, 224706 (2008).
[47]V. S. Bajaj, C. T. Farrar, M. K. Hornstein, I. Mastovsky, J. Vieregg, J. Bryant, B. Eléna, K. E. Kreischer, R. J. Temkin, and R. G. Griffin, J. Magn. Res. **160**, 85 (2003).